Effects of pressure gradients and convection on the inner plasma sheet stability

V. Prosolin, I. Voronkov, and E. Donovan

Abstract: We present a computer model that solves the system of nonlinear MHD equations in dipolar coordinates and is designed specifically to simulate the near-Earth plasma sheet region which has a near-dipolar field line topology. The objective of this work is a detailed study of the inner plasma sheet as a region of particular importance for auroral processes including the proton aurora and near-Earth breakup. Such factors affecting the stability of the inner plasma sheet as Earthward plasma pressure gradients and different patterns of bulk plasma motion are considered. Modeling results show that pressure gradients lead to magnetic field line stretching and increased values of the ballooning instability growth rate. Both Earthward and tailward convection bursts form a local min-B region. However, effects of tailward bursts are stronger. Earthward convection forms a potentially unstable min-B region at about 9 R_E, whereas tailward convection does not have a destabilizing effect.

Key words: Substrom, Ballooning Instability, Modeling, Plasma Dynamics.

1. Introduction

It is generally recognized that the primary mechanism for energy and plasma transport through the magnetosphere is magnetospheric convection. In the magnetotail, plasma travels from the nightside reconnection region towards the Earth until it reaches the region of strong near-dipolar magnetic field - near-Earth plasma sheet.

There is no concensus on some particular details of plasma propagation through the plasma sheet, but it is known that flows can be highly variable – for example, periods of steady convection (e.g., [25]), bursty bulk flows (e.g., [1]), and flow reversals [15], have been observed. The complex dynamics of the plasma sheet have been shown to be closely related to many auroral processes. These include, for example, the proton aurora band at the radial boundary of the auroral region ([21], [22]), which maps to the so-called b2i boundary [6]. Also, the most pronounced field line resonances are observed in this region, owing to sharp radial gradients of magnetic field ([20], [8], [23], [17]). The substorm onset auroral arc intensifies and breaks up in this region ([16], [28], [29]). Therefore, there is substantial evidence that energy transport in the inner plasma sheet plays a crucial role in auroral dynamics.

The main idea of how plasma sheet dynamics can be coupled with auroral features involves the transformation of potential energy stored in the near-Earth magnetosphere into kinetic energy of field-aligned plasma flows affecting the ionosphere ([9], [10]). In order to provide this ionosphere-magnetosphere coupling, a quite fast (of the order of tens of seconds) mechanism of energy transformation is required, so a number of authors have proposed that plasma instabilities takes place. These include the current disruption model ([12], [13], [18]), convection reversal model [15], kinetic ballooning instability [4], shear flow ballooning instability ([24], [27]), and non-linear ballooning instability [5]. Another group of models suggests that a distant magnetotail disruption may trigger the near-Earth energy release and consequent auroral activity when disturbances from the more distant magnetotail reach the inner plasma sheet ([2], [26], [3]). Currently, there is no general public acceptance of either model. However, a common point in all proposed mechanisms is that the sufficient amount of energy must be stored in the inner plasma sheet and one way or another this region should be destabilized (e.g., [29] and references therein). Some aspects of this problem are addressed in this paper.

This study aims to discuss the influence of several factors on the inner plasma sheet stability from the modeling point of view. We use a three dimensional MHD model to simulate the dynamics of the inner plasma sheet for different configurations. In the first part, we perform the stability analysis of plasma sheet configurations with an Earthward pressure gradient present. Different magnitudes of the pressure gradient are tested for the ballooning instability. In the second part, we examine different plasma bulk flow patterns – bursty flows and steady convection. Both tailward and Earthward velocity directions are considered to examine possible destabilization by the convection.

2. Ballooning Instability in the Inner Plasma Sheet

It has been observed that active electron arcs, including the pre-onset arc, are often seen within the region of strong $H\beta$ proton emissions and energetic (tens of keV) proton precipitation at the equatorial edge of the evening sector of the auroral region ([21], [27], [16]). Quite often, Earthward pressure gradients are observed by the satellites crossing or entering the inner plasma sheet at 8-12 R_E ([14], [19]).

A dipolar magnetic field with uniform pressure distribution is an equilibrium configuration. The ballooning instability can occur in a system where the magnetic field is stretched beyond the dipolar shape such that a pressure gradient force is balanced by the Ampere magnetic force (Figure 1).

Under certain conditions, the inner plasma sheet can become ballooning unstable. The following relation for the ballooning

Received 6 June 2006.

V. Prosolin, I. Voronkov, and E. Donovan. Department of Physics and Astronomy, University of Calgary.

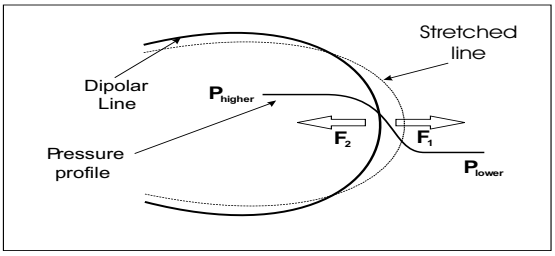

Fig. 1. Two forces in balance - Curvature (F_1) and pressure gradient (F_2).

instability growth rate is derived in [27]:

$$\omega^2 = -\frac{P'_{tot}}{\rho}\left(2(lnB)' - \frac{2P'_{tot}}{\rho V_f^2}\right) \quad (1)$$

where B is the magnetic field, P_{tot} is the total (magnetic plus thermal) pressure, ρ is the plasma density, V_f is the speed of the fast mode, and prime denotes the radial (anti-earthward) derivative. We applied the above formula to data from [11] and identified a potentially unstable region in the vicinity of the strong pressure gradient (Figure 2).

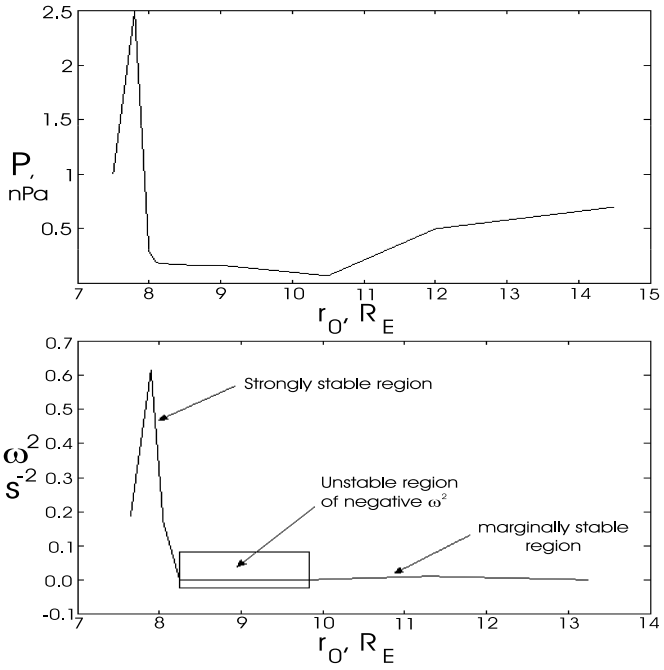

Fig. 2. An observed pressure profile (from [11]) and corresponding ballooning instability growth rate (ω^2) in the equatorial plane.

3. Effects of Earthward Pressure Gradients

As we have shown that a strong earthward pressure gradient can lead to an unstable region, the following question arises – How strong does the gradient need to be in order to lead to a local instability?

Using the abovementioned computer code we have studied evolution of the system with an initially given pressure profile in order to find a possible relation between the magnitude of the gradient and the instability growth rate.

The initial configuration for all the runs discussed in this paper is set as follows, unless otherwise specified:

- Dipolar magnetic field
- Uniform plasma pressure and density distribution:$\rho = 1.67 \cdot 10^{-24} g/cm^3$ ($n = 1\,cm^{-3}$), $P_{max} = 1\,nPa$
- Zero velocity

For the purpose of studying effects of pressure gradients we set the initial pressure profile in the following form:

$$P\,|_{equator} = P_{max}(1 - \frac{\arctan a(r_0 - r_{mid})}{b})$$

where P_{max} is the maximum value of pressure corresponding to the inner boundary, r_0 is a radial distance along the equator, r_{mid} is the center of the pressure gradient, and a and b are coefficients defining the magnitude and width of the gradient.

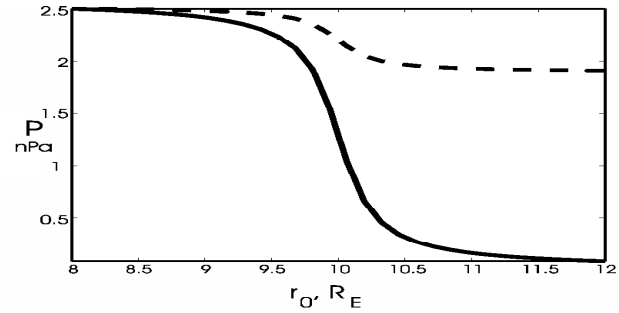

Fig. 3. Initial pressure profiles in the equatorial plane

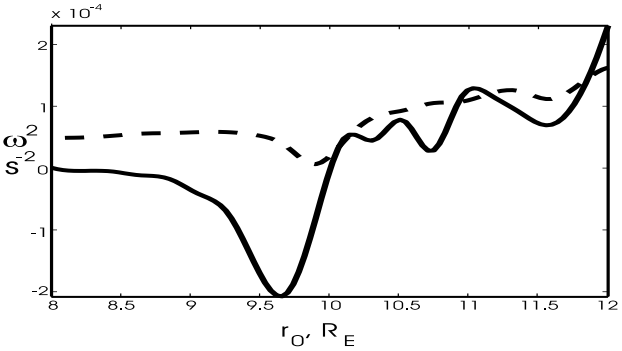

Fig. 4. ω^2 equatorial profile at $t = 50$ seconds

Two sample initial pressure profiles are shown in Figure 3. Since at $t = 0$ the system is not in the equilibrium, a reconfiguration process begins. Modeling shows that in the vicinity of the strongest gradient a region of minimum magnetic field is formed (Figure 5) which corresponds to stretching of the field lines. The stretching increases field line curvature thereby creating the curvature force opposing the pressure gradient force to re-establish plasma equilibrium.

By applying Eq. 1, we obtain equatorial profiles of ω^2 shown in Figure 4. Similarly to the analysis performed with observed

data, we find that the minimum-B region and maximum of the pressure gradient correspond to the minimum in ω^2 marking an unstable region ($\omega^2 < 0$).

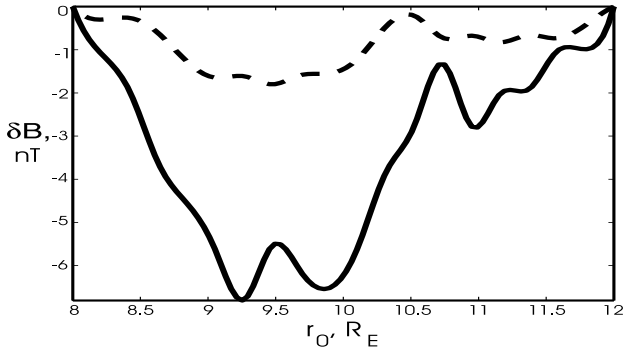

Fig. 5. Magnetic field perturbation profile at the equator at $t = 50$ seconds

As seen in Figures 3 and 4, the maximum magnetic field perturbation and most negative value of ω^2 correspond to the larger gradient. However, it is obvious that the instability can occur only when the pressure gradient overcomes some threshold. In order to verify that, we have performed computer simulations for several different magnitudes of pressure gradients in the range from 0.25 nPa/R_E to 4.4 nPa/R_E.

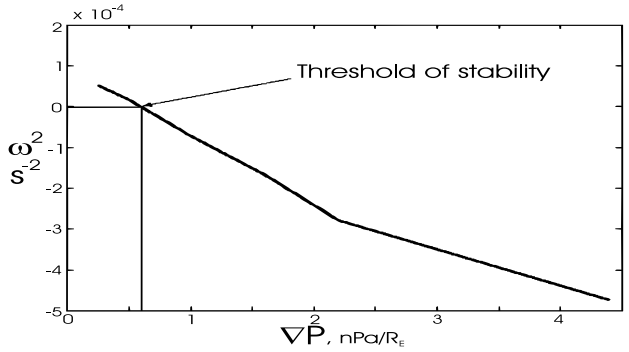

Fig. 6. Ballooning instability growth rate ω^2 vs. plasma pressure gradient ∇P

By plotting the minimum value of ω^2 vs. the magnitude of the initial pressure gradient, we have found the point at which $\omega^2 = 0$ which corresponds to a threshold of the instability. As one can see in Figure 6 the threshold lies at 0.6 nPa/R_E.

4. Bulk Plasma Motion

As noted earlier, convection in the magnetotail occurs in different forms, such as steady convection and "discrete bursts of high-velocity flow of limited spatial extent" [7]. In this secion we describe four different patterns of plasma bulk motion (i.e., convection): flow bursts and steady convection for both Earthward and tailward velocity directions.

4.1. Bursty Flows

In order to model an Earthward moving pulse we set a gaussian profile of radial velocity with the amplitude of 1000 km/sec as shown in Figure 7.

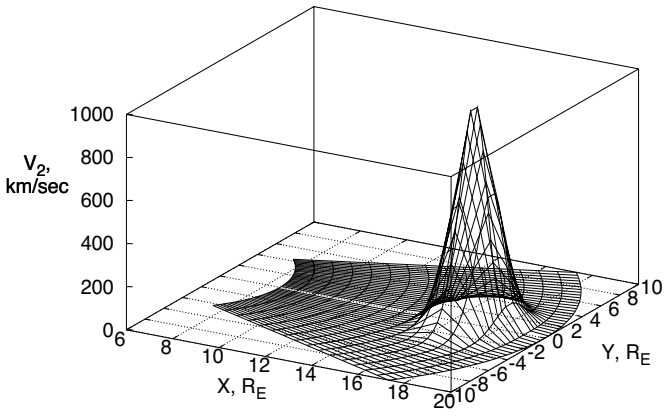

Fig. 7. Earthward pulse: radial velocity equatorial profile at $t = 0$

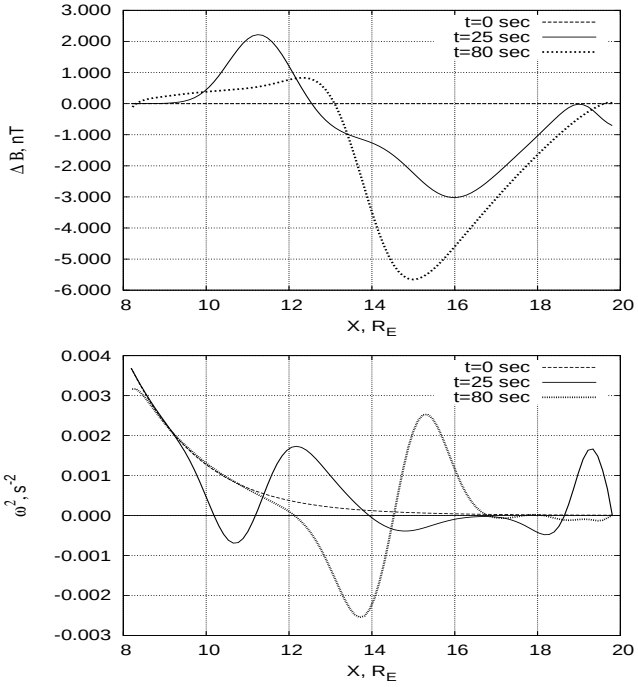

Fig. 8. Earthward pulse: magnetic field perturbation and instability growth rate profiles at different times

We take snapshots of the resulting magnetic field perturbation and ballooning instability growth rate at several moments of time. Figure 8 shows that an Earthward pulse modifies the field configuration so that a min-B region is formed along with a potentially unstable ($\omega^2 < 0$) region in the vicinity of magnetic field gradient.

The effects of a tailward pulse (Figure 9) are almost negligible in comparison with the previous case, as seen in Figure 10. No clear change in magnetic field topology is observed, although at times the system may get into a marginal state - ω^2

is just below 0.

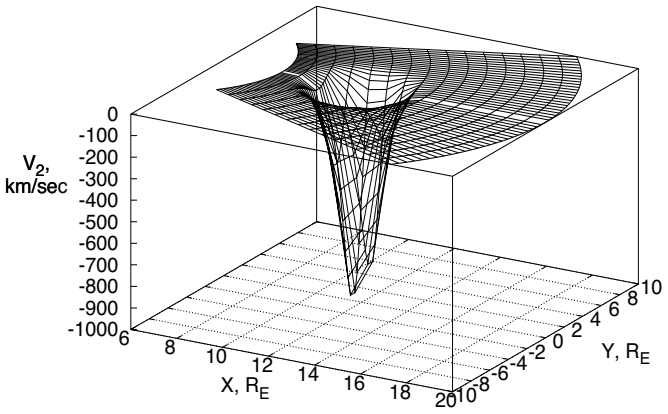

Fig. 9. Tailward pulse: radial velocity equatorial profile at $t = 0$

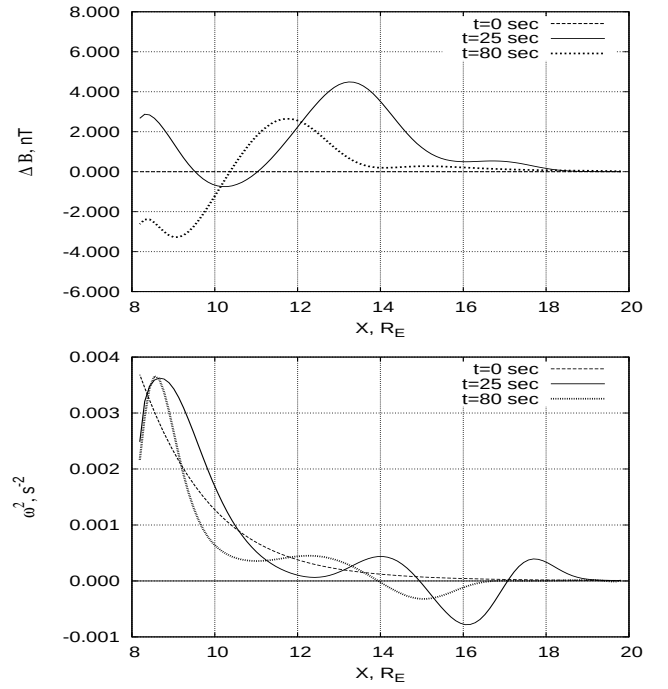

Fig. 10. Tailward pulse: magnetic field perturbation and instability growth rate profiles at different times

4.2. Steady Convection

In an ideal case, the steady convection can be considered an E×B drift, so for a dawn-to-dusk (dusk-to-dawn) electric field plasma will drift Earthward (tailward). Here we consider both directions of electric field.

We start by setting the velocity configuration using $\mathbf{V} = \mathbf{E}\times\mathbf{B}/B^2$ which for dawn-to-dusk electric field gives an equatorial velocity field shown on Figure 11. Since the magnetic field lines are equipotential lines in this case, we can propagate the equatorial profile over the entire three-dimensional computation domain by using the following relations:

$$E_2(x,y,z) = \frac{E_2^{equator} h_2^{equator}}{h_2(x,y,z)}$$

$$E_3(x,y,z) = \frac{E_3^{equator} h_3^{equator}}{h_3(x,y,z)}$$

where $E_2(x,y,z)$ and $E_3(x,y,z)$ are two perpendicular to the magnetic field components of the electric field at a point defined by Cartesian coordinates (x,y,z), $E_2^{equator}$ and $E_3^{equator}$ are the electric field components in the equatorial plane that lie on the same magnetic field line, $h_2^{equator}$, $h_3^{equator}$ and $h_2(x,y,z)$, $h_3(x,y,z)$ are corresponding metrics.

One can notice that for a uniform (in the equatorial plane) electric field, as the dipolar magnetic field increases Earthward, the E×B drift velocity descends.

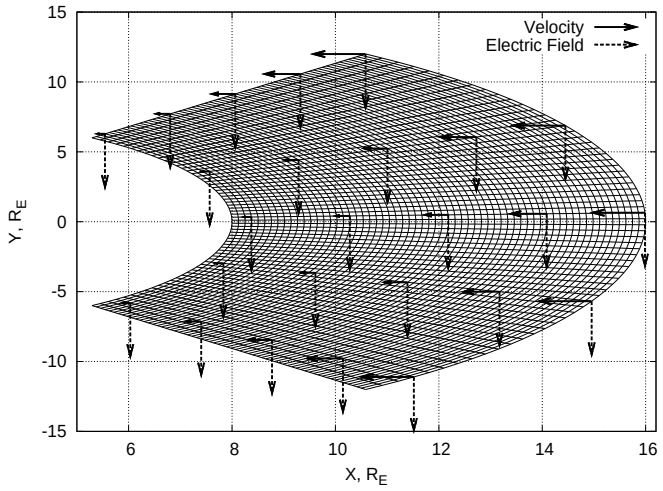

Fig. 11. Electric field and corresponding E×B drift velocity distribution in the equatorial plane shown on the computational grid

In order to study the effect of steady convection, the electric field, and therefore velocity derived from it, at the outer domain boundary is sustained at the initial level to represent a constant plasma inflow from outside. The other boundaries are kept open, i.e. zero gradient boundary conditions are imposed.

Since the initial configuration is not an equilibrium state, the first stage of system evolution includes generation of different compressional wave modes that propagate out of the region through the open boundaries and do not play a role in the subsequent dynamics.

After the first stage, a slow evolution stage - not wave-like, takes place. Figure 12 shows that the magnetic field is carried towards the Earth building up an increased magnetic field at the close radial boundary. We find that under the influence of plasma input, the magnetic field configuration changes in such a way that a local minimum forms between 9 and 10 R_E (see Figure 12) by $t = 140$ seconds of physical time and remains at this level with minor changes until the end of simulation ($t = 250$ seconds). The region of minimum field strength is then found to be potentially unstable with respect to the ballooning mode (Figure 13).

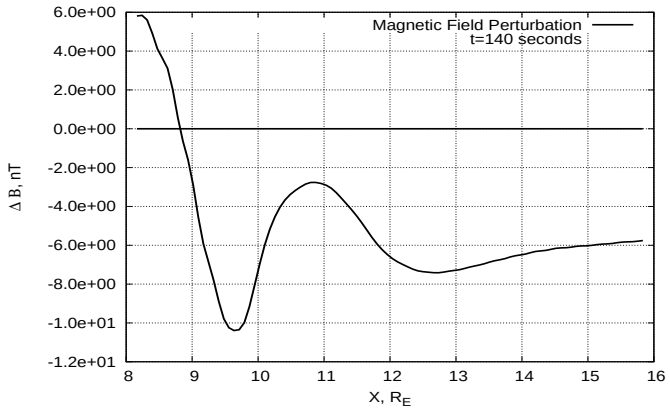

Fig. 12. Magnetic field perturbation at $t = 140$ seconds for the case of dawn-to-dusk electric field

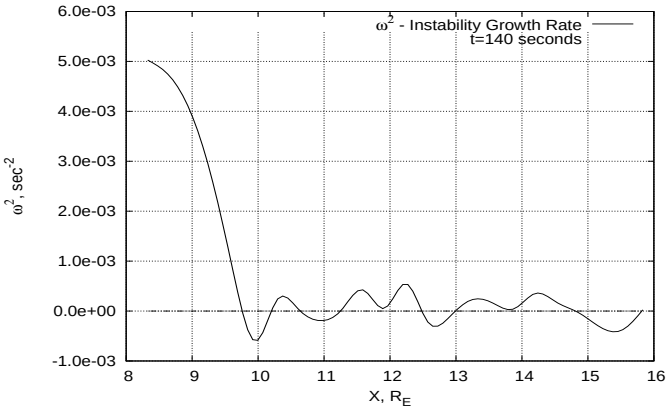

Fig. 13. Instability growth rate at $t = 140$ seconds for the case of dawn-to-dusk electric field

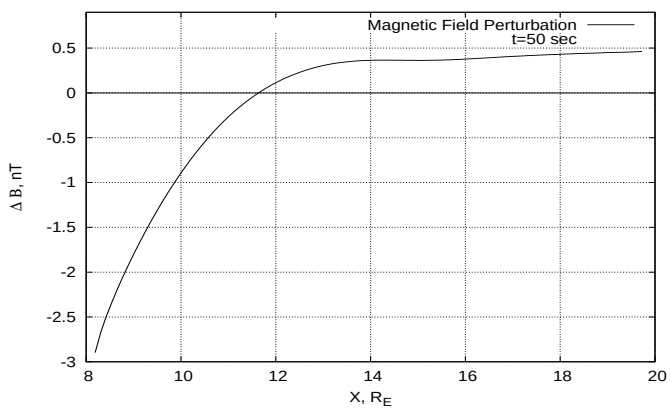

Fig. 14. Magnetic field perturbation at $t = 50$ seconds for the case of dusk-to-dawn electric field

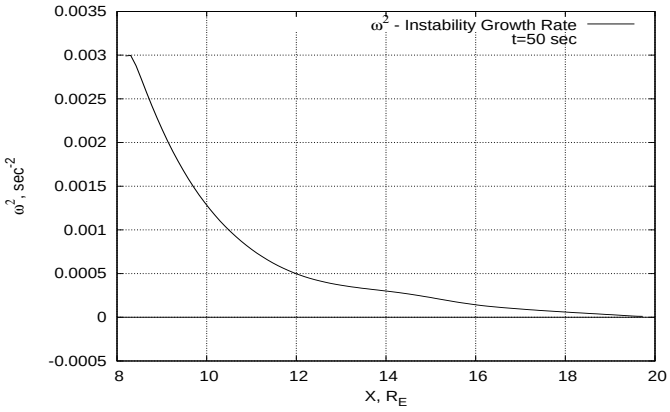

Fig. 15. Instability growth rate at $t = 50$ seconds for the case of dusk-to-dawn electric field

As mentioned above, convection reversals can occur in the near-Earth magnetotail which points to the electric field reversal [15]. As a demonstration of what the inner plasma sheet dynamics may be like in that case, we ran a simulation for a uniform dusk-to-dawn electric field.

Figure 14 illustrates how the magnetic field is driven tailward so that it gradually increases tailward with no destabilizing effect since $\omega^2 > 0$ in the region. (Figure 15).

5. Conclusion

In this paper we have performed a study of different factors that may affect the stability in the inner plasma sheet. We have simulated plasma dynamics in different configurations which include Earthward plasma pressure gradients, Earthward and tailward flow bursts, and convection under the influence of dawn-to-dusk and dusk-to-dawn electric fields.

It has been obtained that Earthward pressure gradients in the inner plasma sheet comparable to observed values lead to magnetic field line stretching and values of the ballooning instability growth rate above the stability threshold. A dependence between the magnitude of the pressure gradient and values of the instability growth rate has been observed and a threshold of stability found from simulations - $0.6\,nPa/R_E$.

The analysis of different bursty flow patterns shows that the ballooning instability can be expected for both Earthward and tailward velocity directions. We have considered two bulk flow types - bursty motion and steady convection. The Earthward flow burst forms a local min-B region where the ballooning instability is possible. The effect of the tailward burst is less significant as it does not lead to a dramatic magnetic field reconfiguration, although the system may reach a marginal stability state.

In the last part, both directions of the cross-tail electric field have been modeled. Earthward convection has been found to form a localized min-B region and provide favorable conditions for development of the ballooning instability. On the other hand, tailward convection does not bring the system to an unstable state.

References

1. Angelopoulos, V., W. Baumjohann,, C. F. Kennel, F. V, Coroniti, M. G. Kivelson, R. Pellat, R. J. Walker, H. Luhr, and G. Paschmann, Bursty bulk flows in the inner center plasma sheet, *Journal of Geophysical Research*, 97, 4027, 1996.
2. Baker, D. N., T. I. Pulkkinen, V. Angelopoulos, W. Baumjohann, and R. L. McPherron, Neutral line model of substorms:

Past results and present view. *Journal of Geophysical Research*, 101:12,975, 1996.
3. Birn, J., M. Hesse, G. Haerendel, W. Baumjohann, and K. Shiokawa, Flow braking and substorm current wedge. *Journal of Geophysical Research*, 104:19,895, 1999.
4. Cheng, C. Z., and A. T. Y. Lui (1998), Kinetic ballooning instability for substorm onset and current disruption observed by AMPTE/CCE, *Geophys. Res. Lett.*, 25(21), 4091–4094.
5. Dobias, P., I. O. Voronkov, and J. C. Samson, On nonlinear plasma instabilities during the substorm expansive phase onset. *Physics of Plasmas*, 11:2046, 2004.
6. Donovan, E. F., B. J. Jackel, I. Voronkov, T. Sotirelis, F. Creutzberg, and N. A. Nicholson, Ground-based optical determination of the b2i boundary: a basis for an optical mt-index. *Journal of Geophysical Research*, 108:1115, 2003.
7. Fairfield, D. H., T. Mukai, M. Brittnacher, G. D. Reeves, S. Kokobun, G. K. Parks, T. Nagai, H. Matsumoto, K. Hashimoto, D. A. Gurnett, and T. Yamamoto, Earthward flow bursts in the inner magnetotail and their relation to auroral brightenings, AKR intensifications, geosynchronous particle injections and magnetic activity, *Journal of Geophysical Research, 104*, 355–370, 1999.
8. Fenrich, F. R., J. C. Samson, G. Sofko, and R. A. Greenwald, Ulf high- and low-m field line resonances observed with the super dual auroral radar network. *Journal of Geophysical Research*, 100:21,535, 1995.
9. Galperin, Yu. I., A. V. Volosevich, and L. M. Zeleny, Pressure gradient structures in the tail neutral sheet as "roots of the arcs" with some effects of stochasticity, *Geophys. Res. Lett.*, 19(21), 2163–2166, 1992.
10. Galperin, Yu. I., An onset development according to the "minimum-B" concept: further analysis, In *Substorms-5, Proceedings of the 5th International Conference on Substorms (ICS-5)*, page 291, Eur. Space Agency Spec. Publ., SP–443, 2000.
11. Kistler, L. M., E. Möbius, W. Baumjohann, and G. Paschmann, Pressure changes in the plasma sheet during substorm injections. *Journal of Geophysical Research*, 97:2993, 1992.
12. Lui, A. T. Y., R. E. Lopez, S. M. Krimigis, R. W. McEntire, L. J. Zanetti, and T. A. Potemra, A case study of magnetotail current sheet disruption and diversion, *Geophys. Res. Lett.*, 15(7), 721–724, 1988.
13. Lui, A. T. Y., A synthesis of magnetospheric substorm models, *Journal of Geophysical Research*, 96(A2), 1849–1856, 1991.
14. Lui, A. T. Y., R. E. Lopez, B. J. Anderson, K. Takahashi, L. J. Zanetti, R. W. McEntire, T. A. Potemra, D. M. Klumpar, E. M. Greene, and R. Strangeway, Current disruptions in the near-earth neutral sheet region. *Journal of Geophysical Research*, 97:1461, 1992.
15. Lyons, L. R., A new theory for magnetospheric substorms, *Journal of Geophysical Research*, 100(A10), 19,069–19,082, 1995.
16. Lyons, L. R., I. O. Voronkov, E. F. Donovan, and E. Zesta, Relation of substorm breakup arc to other growth-phase auroral arcs. *Journal of Geophysical Research*, 107:1390, 2002.
17. Mann, I. R., I. Voronkov, M. Dunlop, E. Donovan, T. K. Yeoman, D. K. Milling, J. Wild, K. Kauristie, O. Amm, S. D. Bale, A. Balogh, A. Vilijanen, and H. J. Opgenoorth, Coordinated ground-based and cluster observations of large amplitude global magnetospheric oscillations during a fast solar wind speed interval. *Ann. Geophys.*, 20:1, 2002.
18. Ohtani, S., F. Creutzberg, T. Mukai, H. Singer, A. T. Y. Lui, M. Nakamura, P. Prikryl, K. Yumoto, and G. Rostoker, Substorm onset timing: The December 31, 1995, event, *J. Geophys. Res.*, 104(A10), 22,713–22,728, 1999.
19. Ohtani, S., K. Takahashi, L. J. Zanetti, T. A. Potemra, R. W. McEntire, and T. Iijima, Initial signatures of magnetic field and energetic particle fluxes at tail reconfiguration: Explosive growth phase. *Journal of Geophysical Research*, 97:19,311, 1992.
20. Ruohoniemi, J. M., R. A. Greenwald, and K. B. Baker. Hf radar observations of pc 5 field line resonances in the midnight/early morning mlt sector. *Journal of Geophysical Research*, 96:15,697, 1991.
21. Samson, J. C., L. R. Lyons, P. T. Newell, F. Creutzberg, and B. Xu, Proton aurora and substorm intensifications. *Geophys. Res. Lett.*, 19:2167, 1992.
22. Samson, J. C. Mapping substorm intensifications from the ionosphere to the magnetosphere. In J. R. Kan, J.D. Craven, and S.-I. Akasofu, editors, *SUBSTORM-2, International Conference on Substorms-2*. Univ. of Alaska, Fairbanks, 1994.
23. Samson, J. C., L. L. Cogger, and Q. Pao, Observations of field line resonances, auroral arcs and auroral vortex structures. *Journal of Geophysical Research*, 101:17,793, 1996.
24. Samson, J. C., R. Rankin, and I. Voronkov, Field line resonances, auroral arcs, and substorm intensifications. In J.L. Horwitz, editor, *Geospace Mass and Energy Flow: Results from the International Solar-Terrestrial Physics Program, Geophys. Monogr. Ser.*, volume 104, page 161. AGU, Washington, D.C., 1998.
25. Sergeev, V. A., R. J. Pellinen, and T. I. Pulkkinen, Steady magnetospheric convection: Review of recent results, Space Sci. Rev., 75, 551, 1996.
26. Shiokawa, K., W. Baumjohann, and G. Haerendel, Braking of high-speed flows in the near-earth tail. *Geophys. Res. Lett.*, 10:1179, 1997.
27. Voronkov, I. O., E. F. Donovan, B. J. Jackel, and J. C. Samson, Large-scale vortex dynamics in the evening and midnight auroral zone: Observations and simulations. *Journal of Geophysical Research*, 105:18,505, 2000.
28. Voronkov, I. O., E. F. Donovan, and J. C. Samson, Observations of the phases of the substorm. *Journal of Geophysical Research*, 108:1073, 2003.
29. Voronkov, I. O., E. F. Donovan, P. Dobias, V. I. Prosolin, M. Jankowska, and J.C. Samson, Late growth phase and breakup in the near-earth plasma sheet. In *Proceedings of the 7th International Conference on Substorms (ICS-7)*. 140, 2004.